Stable operation process of earthquake early warning system based on machine learning: trial test and management perspective

Jae-Kwang Ahn[1], Euna Park[2], Byeonghak Kim[2], Eui-Hong Hwang[2] and Seongwon Hong[3]*

[1]Earthquake and Volcano Techonlogy Team, Korea Meteorological Administration, Seoul, Republic of Korea, [2]Earthquake and Volcano Research Division, Korea Meteorological Administration, Seoul, Republic of Korea, [3]Department of Safety Engineering, Korea National University of Transportation, Chungju-si, Chungbuk, Republic of Korea

Earthquake Early Warning (EEW) is an alert system, based on seismic wave propagation theory, to reduce human casualties. EEW systems mainly utilize technologies through both network-based and on-site methods. The network-based method estimates the hypocenter and magnitude of an earthquake using data from multiple seismic stations, while the on-site method predicts the intensity measures from a single seismic station. Therefore, the on-site method reduces the lead time compared to the network-based method but is less accurate. To increase the accuracy of on-site EEW, our system was designed with a hybrid method, which included machine learning algorithms. At this time, machine learning was used to increase the accuracy of the initial P-wave identification rate. Additionally, a new approach using a nearby seismic station, called the 1+ α method, was proposed to reduce false alarms. In this study, an on-site EEW trial operation was performed to evaluate its performance. The warning cases for small and large events were reviewed and the possibility of stable alert decisions was confirmed.

KEYWORDS

earthquake early warning, on-site, stable operation, trial test, machin learning

1 Introduction

When an earthquake occurs, the earthquake early warning (EEW) service rapidly detects and analyses the P-wave and transmits warning messages to the public. The pre-hazard early warning system plays a role in disaster prevention in cities (Eichenberger et al., 2013; Liu et al., 2021). The EEW has been proven to be highly effective in reducing human casualties since the 2000s (Allen and Melgar, 2019). The aim of EEW is to notify the public about imminent strong ground shaking and to protect the people, public systems, and national infrastructure (Heaton, 1985; Strauss and Allen, 2016; Allen and Melgar, 2019). Therefore, EEW systems were operational or/and being tested in over 20 countries (Cremen and Galasso, 2020). In the United States (Bostrom et al., 2022), Mexico (Santos-Reyes, 2019; Vaiciulyte et al., 2022), Japan (Doi, 2011; Nakayachi et al., 2019, Peru (Bossu et al., 2022) New Zealand (Becker et al., 2020), and Italy (Satriano et al., 2011), EEW is known to have a high public perception for its usefulness.

The relevant societal aspects related to EEW systems have been highlighted (Dallo et al., 2022). Thus, the operator considers the propagation system, the thought process about the

system setting for alert, and the importance of actionable message content. Currently, the purpose of EEW is 1) to provide the necessary information to warn the public and respond to actions; 2) to lead to safety for populations at risk of imminent threats using the messages; and 3) to minimize response delay (National Academies of Sciences, 2018). However, the decision-making of EEW alert speed is more important than the transmission of this information. Therefore, many studies have attempted to reduce the lead-time of EEW (Picozzi et al., 2015). The Korea Meteorological Administration (KMA) conducts a network-based EEW service for earthquakes and has recognized the limitations of this technology in shortening warnings. Therefore, KMA has recently promoted research on an on-site warning method and is currently trial testing it.

EEWs are developed based on two approaches: the network-based method (Chen et al., 2015; Colombelli et al., 2015; Behr et al., 2016; Chung et al., 2019) and the on-site method (Hsiao et al., 2009; Parolai et al., 2015; Caruso et al., 2017; Spallarossa et al., 2019). Network-based EEWs are used worldwide, which estimate the hypocenter and magnitude of an earthquake using the time and amplitude of P-waves at multiple seismic stations. A warning is issued if the estimated magnitude exceeds the threshold set by each country or region through an automatic process. The propagated seismic intensity measures (IMs) in each area using ShakeMap (Verros et al., 2017), from the estimated magnitude and hypocenter, can be predicted. However, network-based EEW requires data from several observatories (at least three) to determine the hypocenter and magnitude. Therefore, EEW takes several seconds to make a warning decision after the occurrence of an earthquake. However, owing to this time required for a warning decision, certain areas, called the "blind zones," are affected by the earthquake even before the alarm is triggered (Caruso et al., 2017). Furthermore, the time from a large seismic ground motion to the alarm is termed the "lead time" (Cremen and Galasso, 2020). The mission of EEW development is to increase accuracy while reducing lead time. However, this leads to errors in hypocenter information, increasing the incidence of false alarms (Allen and Melgar, 2019).
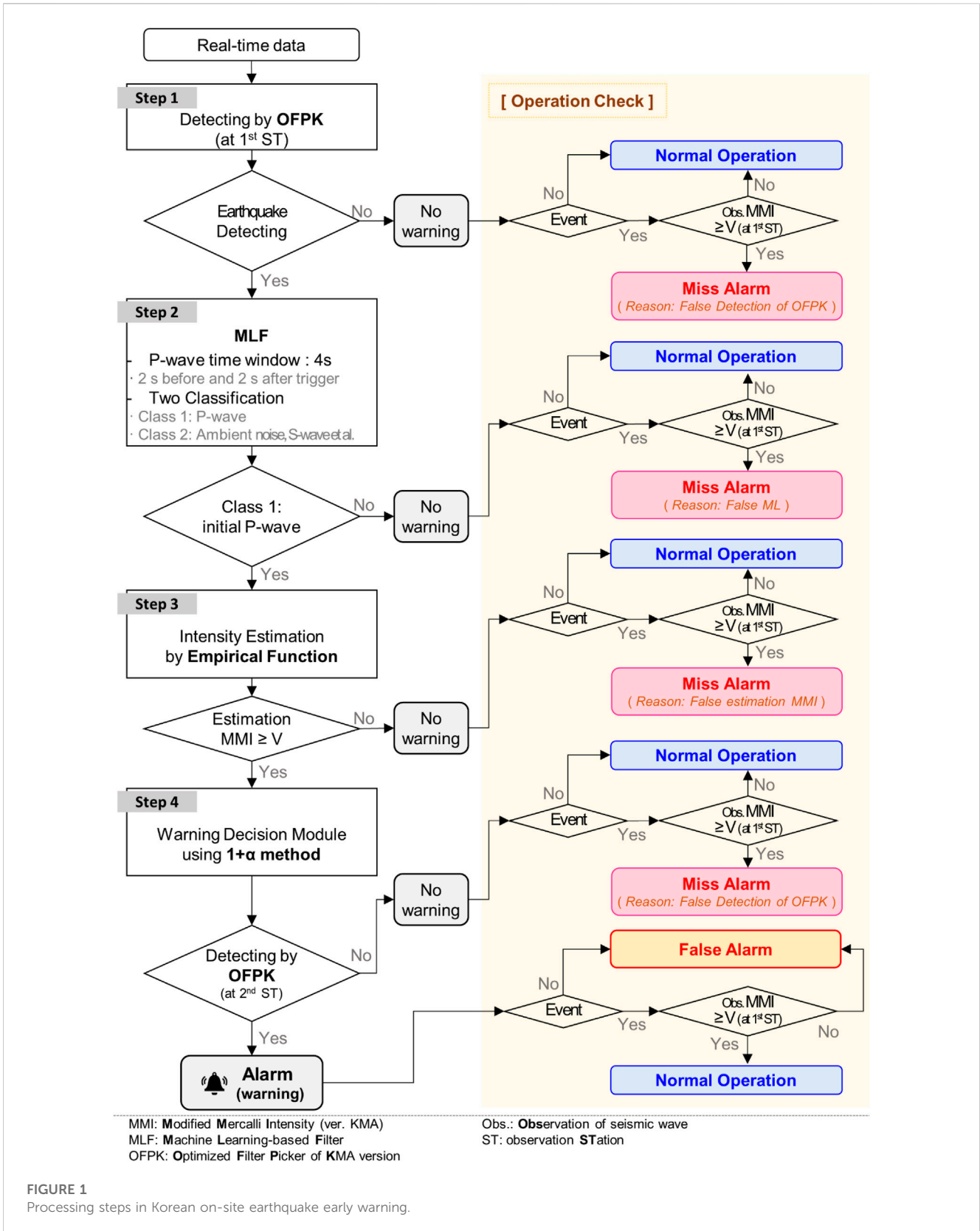
The on-site EEW is based on data from a single seismic station, which predicts the IM from the P-wave first motions without estimating the magnitude and location of the earthquake. Nakamura's Urgent Earthquake Detection and Alarm System (UrEDAS) earthquake warning system (Nakamura, 1988; Nakamura et al., 2011) can be considered an early version of this on-site EEW. UrEDAS is an earthquake disaster prevention system with an automatic train controlling system for the Seikan undersea tunnel and Shinkansen lines (Nakamura and Saita, 2007). This method only requires the P-wave first motion information from a single seismic station; therefore, the lead time is reduced more than that of network-based EEW. In addition, on-site EEW can be used for buildings (Ventura et al., 2019), structures (Bindi et al., 2016), schools, and specific areas (Wu and Mittal, 2021) because the system alone operates without a network. However, the on-site EEW can produce false and missed alarms due to its lower accuracy compared to the network-based EEW, making it difficult to use for public service in smart cities. Therefore, EEW decision-making strategy, should be set off with the lowest missed-alarm and false-alarm probabilities operated (Wang et al., 2018).

Artificial intelligence (AI) and big data technologies have become increasingly important in the field of environmental management and disaster mitigation (Zhang and He, 2020). This underscores the importance of exploring new and innovative ways to integrate these technologies into early warning systems for natural disasters. One of the primary components of EEW systems is the rapid detection and identification of seismic waves. However, traditional methods based on empirical elements and characteristic patterns [e.g., short-term average and long-term average (STA/LTA) (Allen, 1982) and filter-picker (Lomax et al., 2012)] have limitations in terms of accuracy. This has led researchers to explore the potential of machine learning (ML)-based technology as a replacement for these conventional methods in earthquake detection [e.g., CRED (Mousavi et al., 2019), DetNet (Zhou et al., 2019), DPick (Yanwei et al., 2021), EQTransformer (Mousavi et al., 2020), Yews (Zhu et al., 2019)]. The use of ML-based detect models has shown higher accuracies in earthquake detection than traditional models such as the detection of STA/LTA and filter-picker. However, it should be noted that ML-based models require a time window of >2 s for several reasons. Firstly, convolutional and/ or recurrent neural networks extract semantic features from images of waveform and frequency characteristics, which requires a longer time window to capture sufficient information. Secondly, as mentioned previously, earthquakes may be underestimated when applying a short P-wave time window, as the characteristics of P-waves are not properly taken into consideration. Therefore, it has been difficult to apply EEWs as they must rapidly and reliably discriminate event signals within a few seconds (Meier et al., 2019).

Another challenge in the field of EEW is the implementation of AI for the entire system, which is shown represent research to as Deepshake (Datta et al., 2022). This technology not only detects earthquakes but also provides source information, such as magnitude and hypocenter, based on AI, thereby supporting decision-making for alarms. However, as noted by Datta et al. (2022), perfect detection and rapid analysis cannot be guaranteed due to several factors. Firstly, ML models heavily rely on training data established from previous seismic events, which may not accurately represent future events. Secondly, specific propagation wave properties are challenging to consider in ML models because they are influenced by site and path effects. Thirdly, the seismic wave collection time window required to detect using ML still needs to be reducing. Consequently, no public on-site EEW service has been operated using AI-based systems yet.

Our goal was to combine the strengths of existing technologies for rapid EEW. The Korea Meteorological Administration (KMA) tried to complement on-site warning, which was based on a single station. To achieve this, KMA utilized an ML-based earthquake identification method to increase the accuracy of detecting P-waves. However, this method did not completely filter out artificial waves that were similar to seismic waves. Additionally, KMA introduced a secondary detection network, called "α," to improve detection accuracy. ML-detection requires a minimum of 2 s of seismic wave collection time, and it was possible to detect nearby seismometers during this period. So, KMA included the presence or absence of seismograms from this period in our alert decision-making process.

The South Korean seismic observation network uses seismometers that are located within 14 km of each other because nearby seismographs can detect the P wave within 2 s in the case of

FIGURE 1
Processing steps in Korean on-site earthquake early warning.

an earthquake occurring inland. This helps to reduce the false alarm rate even if ML-based seismic detection misinterprets a non-earthquake signal as an earthquake, by relying on detection at a nearby observatory. The resulting technology is called the Korean on-site (KOS) EEW (Seo et al., 2021a). KOS combines a deep learning model with the initial P-wave detector after the filter-

TABLE 1 Count of decision cases for KOS EEW.

Parameter		Filter-picker	
		Lomax	OFPK[a]
T_{filter}	Filter window	0.865 s	0.108 s
T_{long}	Long term window	12 s	10 s
S_1	Threshold of characteristic function (CF)	9.36	10.36–20.36
S_2	Integral of CF exceeds the value	9.21	10.32–20.32
T_{up}	Time window used for pick validation	0.388 s	0.359–1.759

[a]OFPK: Optimized filter-picker for the Korean Peninsula.

picking step to increase the accuracy of event detection in a single station. IMs are estimated based on the passed P-wave. Subsequently, the earthquake was identified from the signal of a passing filter picker at the nearby observation station. This method is known as the 1+ α method (Seo et al., 2021b, Korean Patent No. 10-221818), which increases the accuracy of event warning determination. In KOS, " α " refers to any device or system that can detect earthquakes, but this study is defined as only KMA seismic stations that have passed stable operation conditions.

In this study, the literature related to the KOS EEW, the ML-based filter (MLF), and outfitting model were thoroughly investigated and systematically summarized. Subsequently, to evaluate the stable alert decisions and performance, real-time tests were conducted by the KMA. This study is extremely significant because real-time operation cases of on-site warning technology are also very limited. Finally, the KOS EEW was inspected in real-time for normal, missed, and false operations, as a public service in Korea.

2 Methodology

2.1 Korean on-site earthquake early warning

Figure 1 illustrates the procedure of the KOS EEW based on Korean Patent No. 10-221818 (Seo et al., 2021b). To avoid triggering an alarm in response to a non-earthquake signal or weak seismic intensity, the system includes four filtering steps. The first step triggers the earthquake signal, and the Step 2 identifies whether the triggered signal is an initial P wave or not, using an ML-based learned filter. Up to the Step 2, the focus is on detecting the initial P-wave of seismic waves. The third step determines the seismic intensity, which is an area that the user can select. The fourth step is an empirical determination of the appropriateness of a signal that has passed the previous steps base on an α station. When KOS EEW issues an alert, it means that the seismic waves are strong enough to potentially cause damage in the target region. However, it is challenging to achieve perfect performance with only a small number of sensors. Therefore, the trial operation system records data according to predetermined procedures and evaluates each stage of the alarm judgment. In this chapter, a detailed description of each step is described.

The Step 1 of the KOS EEW is the triggering stage, in which the P-phase is picked because the picking time is the start of signal

analysis. Traditional triggering modules, such as STA/LTA (Allen, 1982) and filter-picker (Lomax et al., 2012; Fujinawa and Noda, 2013; Mittal et al., 2019), were employed. STA/LTA detects a sudden increase in amplitude of a large signal generated for a short time compared to the normal average amplitude. The filter-picker method additionally used a characteristic function of the signal in which was amplitude for each period. So, earthquakes and artificial noise have different characteristics for each period, making filter-picker method more accurate than the STA/LTA. For the Korean Peninsula, the optimized filter-picker of KMA version (OFPK) sets a time window of 0.5 s immediately after the P-wave is triggered. Table 1 summarizes the threshold of the characteristic function of OFPK.

The Step 1 of KOS EEW acts as a trigger to mark the start of the system's operation. However, it is not perfect and only indicates that a signal has suddenly occurred. For accurate alarm production, further confirmation is needed to ensure that the signal is indeed a seismic wave. This is done by collecting more seismic waves over time after being triggered and checking if they are correct based on the seismic waves collected for a certain period. To enhance the identification rate of seismic signals and improve the accuracy of the alarm, an ML-based filter was included in the Step 2 (Figure 2). Although the Step 1 and Step 2 could be combined from the viewpoint of P-phase picking accuracy, the system has divided the step as ML-based P-wave identification requires an additional 2 s after P-wave triggering. In the Step 2, we could filter out both of the S-wave by earthquake and the noise. Thus, the resulting signal can be only identified as the P-wave of the earthquake.

In the Step 3, KOS EEW determines the alarm based on the predicted seismic intensity. The predicted intensity measure (IM) is calculated from the initial P-wave using an empirical model developed by Lee et al. (2020), which is based on Kanamori's method (Kanamori, 2005). At this time, the initial P-wave amplitude in the vertical direction (i.e., displacement, velocity, acceleration) during a 2 s time window (in Step 2) is calculated. Then, the peak ground velocity (PGV) of the entire seismic record is estimated. The empirical formula proposed by Lee et al. (2020), as follows:

$$log\,(PGV) = 1.885 + 0.905 \cdot log\,\,(P_d) \qquad (1)$$
$$log\,(PGV) = 0.765 + 1.302 \cdot log\,\,(P_v) \qquad (2)$$
$$log\,(PGV) = -1.038 + 1.001 \cdot log\,\,(P_a) \qquad (3)$$
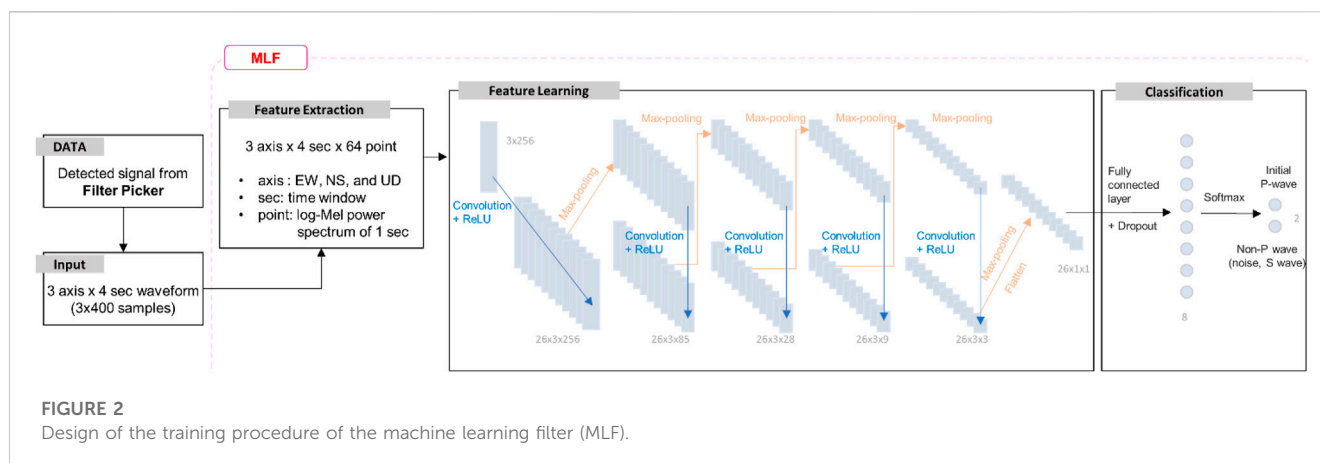
where P_d, P_v, and P_a are the maximum displacement, velocity, and acceleration values of the initial P-wave, respectively. The final PGV is calculated as the arithmetic mean of the three values and converted into IM following the modified Mercalli intensity (MMI) of the KMA.

$$MMI_{KMA} = 2.1939 \cdot log\,(PGV) + 5.0918\,(MMI: I - V) \qquad (4)$$
$$MMI_{KMA} = 2.4686 \cdot log\,(PGV) + 5.0996\,(MMI: V - VIII) \qquad (5)$$

A warning was determined following the MMI_{KMA} estimated using Eq. 4 and Eq. 5. At this stage, KOS EEW sets an alarm based on the operator's desired IM or MMI threshold.

The Step 4 involves considering the pass of OFPK from a nearby seismic station to control false alarms that may occur due to uncertainty in seismic/non-seismic event judgment. During the 2 s delay in issuing the warning in the Step 2, a new nearby

FIGURE 2
Design of the training procedure of the machine learning filter (MLF).

station can be added to detect the signal. The total analysis time theoretically takes 3 s less, comprising 2 s after picking and 1 s less required for calculation up to Step 3. Given the dense seismic observation network on the Korean Peninsula within a radius of 14 km, the P-wave can reach the next station within the time required for analysis by the first station, confirming the warning within the 3 s required for on-site EEW using observation from the nearby station.

In an optimal case, if the record is collected for 2 s at the first station, the first step will be operated at the neighboring station. If the data is delayed or the detection fails, the system waits for detection from a nearby observatory. Therefore, if the initial detection is defined as first detection and active station (FDAS), the conditions for α are 1) Stations within 2–40 km apart from FDAS; 2) Operates for 4 s based on FDAS detection time (KMA, 2022).

After determining the FDAS in the KOS EEW system, any subsequent detection stations will be considered as α stations. This means that any observatory on the operating seismic network can become an α station based on the conditions of the fourth step. This approach ensures that only one alarm is produced for each earthquake, thereby controlling the occurrence of simultaneous multiple alarms. Moreover, the KOS EEW aims to issue warnings within 5 s of the initial observation, with any warnings issued after 5 s being the main rule for the KMA's network-based EEW. This strategy enables the system to operate on-site and network simultaneously.

2.2 Judgment of management perspective

It is important to note that during the test operation, we checked each step of the procedure sequence to ensure that the system was functioning properly. The judgment criteria from a management perspective were also considered to ensure that the system was not generating false alarms or missing alarms. We summarized the management perspective judgment criteria based on the procedure sequence, and the yellow box on the right in Figure 1 illustrates these criteria.

Non-earthquake signals, such as artificially generated signals, blasting, and mechanical anomalies, can pass through to Step 4. If a

warning is triggered by a non-earthquake signal, it can be defined as a false alarm. On the other hand, a false alarm can also be caused by small seismic waves which was a failure of the seismic intensity prediction. In addition, even a strong wave (i.e., MMI is over V, IM induced damage by shaking) may not pass Step 1 to Step 4, and in this case, it can be defined as a missed alarm because the alarm did not sound.

Normal alarms are determined after a series of processes, which include signal detection via OFPK, P-wave picking using MLF, passing the warning intensity thresholds, and signal detection at nearby stations within 4 s. If non-earthquake signals are blocked normally, it is considered normal operation. When a strong wave is transmitted due to an earthquake, and an alarm is issued, this is also considered normal operation. It was mentioned that an error of 1 grade (MMI) is an acceptable level for users, and permitted alarms were defined accordingly.

2.3 Design of machine learning filter

Recently, hazard prediction field has being used ML based on the empirical relationship which was images, signal, and big data (He et al., 2020; Ozsagir et al., 2022; Aminpour et al., 2023). However, due to the mathematical complexity of these models, human empirical decisions are still required for assistance in some cases. Seismic wave phase picking is an example in seismology that requires human assistance. Therefore, many researchers have focused on signal detection-based ML, which requires high accuracy (Zollo et al., 2014; Parolai et zl., 2017; Meier et al., 2019; Mousavi et al., 2019; Zhou et al., 2019; Zhu et al., 2019; Mousavi et al., 2020; Yanwei et al., 2021; Datta et al., 2022). Our system also aimed to accurately detect the initial P-wave using MLF in KOS EEW, which identifies signals within the first 2 s from the arrival of the seismic wave. The MLF is included in the next stage, and the schematic diagram of the training procedure is shown in Figure 2.

To develop MLF (Lee, 2020; Seo et al., 2021a), the following steps were systematically performed:

1) 3-component waveforms of 4 s were collected based on the detected signal from Korean Peninsula. The time at which the

TABLE 2 Convolutional neural network.

Layer	Filter × column × row	Filter (kernel) size	Pooling size	Weights	Biases
Input	1×3×256	-	-	-	-
Conv_1	26×3×256	3×3	-	234	26
Pool_1	26×3×85	-	3	-	-
Conv_2	26×3×85	3×3	-	6,084	26
Pool_2	26×3×28	-	3	-	-
Conv_3	26×3×28	3×3	-	6,084	26
Pool_3	26×3×9	-	3	-	-
Conv_4	26×3×9	3×3	-	6,084	26
Pool_4	26×3×3	-	3	-	-
Conv_5	26×3×3	3×3	-	6,084	26
Pool_5	26×1×1	-	3	-	-
Flatten	26	-	-	-	-
Dropout	26	-	-	-	-
FCL[a]	8	-	-	208	8
Output	2	-	-	16	2
Total parameters					24,934

[a]FCL: fully connected layer.

initial P-wave was detected was called the picking time. The data length was 4 s around the picking time (i.e., picking ±2s). The training dataset comprised two horizontal components and one vertical.

2) The training data were transformed to the log-Mel power spectrum. In the frequency domain analysis, data were processed in 1s. Features with a frequency and amplitude of 64 points were constructed. The extracted feature size of the input data was 768 (3 axis × 4s × 64 points).

3) Feature learning was designed to perform convolutional operations, ReLU activation functions, and max pooling five times, repeatedly.

4) The proposed model was designed to spread the features obtained in previous step to the fully connected layer to identify the P-wave, S-wave, and background noise, and finally assigning them to three classes using the dropout and softmax functions.

The convolutional neural network (CNN) was applied, as summarized in Table 2. Data from the local seismic network from January 2015 to March 2020 was employed, comprising 727 local earthquakes with a magnitude of ≥2.0 and 103 large teleseismic records. 1,734 events from Taiwan were used due to the non-sufficiency of the Korean data. Micro earthquakes were also included to increase the trigger accuracy (Lee, 2020). Thus, 2,564 earthquake data were employed.

To identify earthquakes and non-earthquakes, a dataset dividing the P-wave and S-wave sections in the earthquake record was developed. Non-natural earthquakes (e.g., resulting from fallen earthquakes, nuclear tests, and explosions) and noise data were added to enhance the identification rate. Thus, 3,189,583 sample data were developed.

To verify the performance of the model, the dataset was divided into training sets (1,826,357) and demonstrated test sets (1,363,226) (Seo et al., 2021a). However, models trained directly with this dataset showed an exponential decrease in P-wave detection accuracy with longer learning times. The reason for the decrease in performance was that, in machine learning, the model was overfitted for training data. Therefore, overfitting is a critical concern in machine learning as it pushes the optimization boundaries too far and leads to a decrease in the model's overall performance.
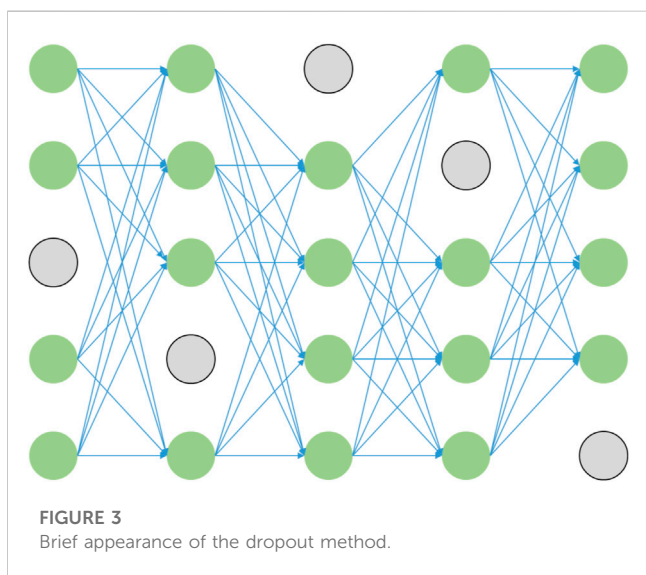
2.4 Troubleshooting for overfitting of MLF

When a model is overfitted to the training data, its performance on new and unseen test data may suffer, despite achieving high accuracy on the training data. This is often due to the model being optimized for noise properties that are specific to the training dataset. To address overfitting, the following three approaches were employed.

Firstly, P-waves, S-waves, and large noise samples, as well as balanced volumes, were augmented. The data-driven ML model learns specific patterns from a given dataset by itself. However, to achieve an optimally trained ML model, a vast amount of training data on earthquake records was needed. Insufficient data may cause misgeneralized predictions on new input data, resulting in overfitting. During the development of MLF, 2,564 earthquakes were used. As there were multiple records observed at various observatories per earthquake, there were 81,394 wave forms. This accounts for only 2.6% of the total dataset, indicating a severe data imbalance that needed to be solved. Therefore, Lee (2020)

TABLE 3 Balanced data set for MLF (Lee, 2020).

	Initial P wave of earthquake	Non-detecting signal of MLF		
		S wave of earthquake	Noise (non-event signal)	Special (i.e., sinking and blasting event)
Training set	1,544,998	196,715	2,299,288	22,905
Test set	1,053,709	165,218	1,616,059	30,120

FIGURE 3
Brief appearance of the dropout method.

performed learning by repeatedly using existing seismic data while varying the data-cutting section based on the original data.

Although this method may not be appropriate in terms of data learning, we used it empirically because there is still a limit to using artificial seismic waves. To solve this problem, we balanced the data by duplicating and adding P-waves, S-waves, and large noise samples to the training and test sets (Lee, 2020). As a result, the learning of MLF increased the number of training and test samples to 4,063,907 and 2,865,106, respectively. Table 3 shows the number of data configured for data learning. Although there was still a data imbalance in the training set, the test set was configured to keep the number of data as similar as possible.

Second, dropout is a method of randomly dropping neurons in the hidden layer according to a preset ratio to limit participation in neural network training. For example, in Figure 3, only 80% of neurons are involved in learning, according to the hyperparameters of the predetermined dropout rate of 0.2 when training the neural network model. It avoids the problem of the artificial neural network model depending on several neurons in a specific layer. It also improves the learning stability of the MLF model and reduces the probability of the model being overfitted to the training data.

Third, the *global* loss function through weight regularization to prevent overfitting was reconstructed. MLF applied the *sigmoid* activation function Eq. 6 to the output of CNN to convert it to a normalized value between 0 and 1 for P-wave classification. A *global* loss function was then used to express the difference between the two *sigmoid* transform values, P-wave and non

P-wave, as a binary cross entropy (*BCE*) loss Eq. 7 (Yeung et al., 2022). However, this function cannot prevent overfitting if the amount of training data is insufficient or the learning proceeds too long. Generally, ML models are trained to perform well on new data (test data), rather than the training data. Therefore, the loss function, which is the learning criterion of the model, needs a trick to 'regulate' the model to prevent its complex fitting to training data and overfitting in the learning process. L2 regularization is a weight regulation technique using L2-norm Eq. 8, one method for calculating the size of a vector. In this study, a *global* loss function was constructed to learn the P-wave detection model by adding a L2 regularization function to the loss function comprising the existing *BCE*. The L2 regularization function prevents our model from being too limited to training data to cause overfitting and increases versatility by establishing a hyper parameter λ that regulates the relative proportions of learning and regulation of the data Eq. 9.

$$f_{sigmoid} = \frac{1}{1 + e^{-(xw+b)}} \quad (6)$$

where x is the input vector data; w is the weight vector; b is scalar value of bias.

BCE loss, which measures the difference between P-waves and non-P-waves based on the information or entropy, can be expressed using the *sigmoid* function as follows:

$$L_{BCE} = -\frac{1}{n}\sum_{i=1}^{n}\left[y_i log\,\sigma(x_i) + (1-y_i)log(1-\sigma(x_i))\right]$$
$$= -\frac{1}{n}\sum_{i=1}^{n}\left[y_i log\left(\frac{1}{1+e^{-(xw+b)}}\right) + (1-y_i)log\left(1-\left(\frac{1}{1+e^{-(x2+b)}}\right)\right)\right] \quad (7)$$

where i is an index of the input data; n is the number of input data; x_i is the i-th input sample; y_i is the target label of x_i

$$L2_{norm}(w)\|w\|_2 = \sqrt{w_1^2 + w_2^2 + \cdots + w_n^2} \quad (8)$$

For computational convenience, the *global* loss function of the model was reconstructed by eliminating the square root of the $L2_{norm}$ and adding the regularization adjustment parameter λ, as follows:

$$L_{global} = L_{BCE} + \frac{\lambda}{2}L_R = L_{BCE} + \frac{2}{\lambda}\left(w_1^2 + w_2^2 + \cdots + w_n^2\right)$$
$$= -\frac{1}{n}\sum_{i=1}^{n}\left[y_i log\left(\frac{1}{1+e^{-(xw+b)}}\right) + (1-y_i)log\left(1-\left(\frac{1}{1+e^{-(xw+b)}}\right)\right)\right]$$
$$+ \frac{\lambda}{2}|w|^2 \quad (9)$$

By applying the above approaches, the accuracy of P-wave detection through the MLF increased to approximately 98.65% after passing through the filter.
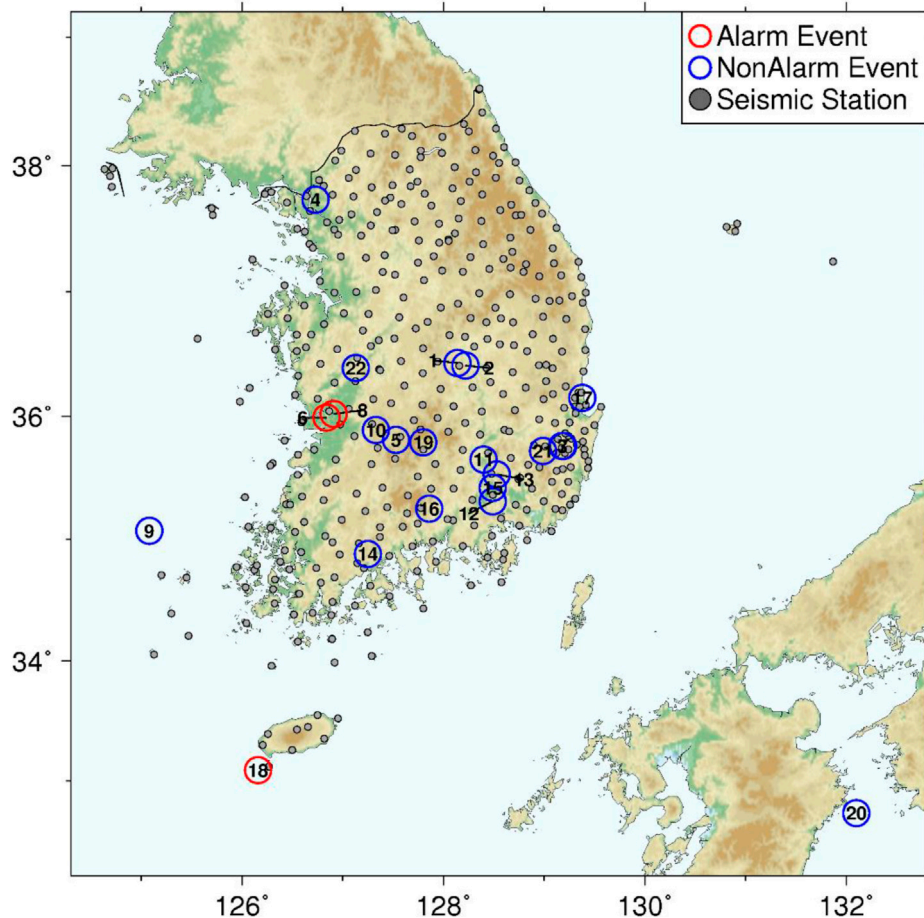
FIGURE 4
Korean on-site earthquake early warning trial operation results from 10.08.2020 to 03.31.2022. Gray circles indicate seismic stations, and red and blue open circles indicate earthquakes for which warnings have been issued and have not been determined, respectively.

3 Implementation of real-time trial operation

We performed an extensive review of the simulation for KOS EEW before the Trial Test. The result of simulations of 69 historical earthquakes was summarized in Supplementary Appendix S1 (KMA, 2022). The simulations resulted in 12 successful alarms, 3 false alarms, and 2 missed alarms, confirming the feasibility of the technology. However, we acknowledge that simulations have limitations in accounting for communication delays, data loss, and unknown noise (i.e., non-earthquake signals). We only showed the false alarm due to overestimated. For simulations, it is difficult to determine "false alarm" for non-earthquake signals. Therefore, a trial operation is necessary to further evaluate the technology's effectiveness in real-time operation.

The model performance was analyzed using earthquakes from 10-08-2020 to 03-31-2022. Initially, events were selected considering possible triggering warnings about the on-site warning issuance criteria. Earthquakes that met one or more of the following conditions during the study period were selected:

1) M_L ≥2.5 that occurred in Korea, 2) earthquakes with a maximum intensity of IV or greater, and 3) tremors felt. In addition, two cases were included in the analysis. The first one was an M_L 6.7 earthquake that occurred in the sea of Oita Prefecture (Kyushu), Japan, in January 2022, which transmitted vibrations to the Korean Peninsula and recorded a maximum seismic intensity III. This earthquake was included to examine the possibility of on-site warning of a teleseismic earthquake. The second one was a false alarm case for a non-seismic event. During the trial operation, most warnings relating to non-seismic events did not pass through the four steps in KOS EEW. However, there was one case of a warning decision made for a non-seismic event. Figure 4 and Table 4 show the distribution of 22 events used for the on-site EEW analysis over the seismic stations. The warning threshold applied to the KOS EEW was V on the MMI scale, rounded off after the PGV calculation.
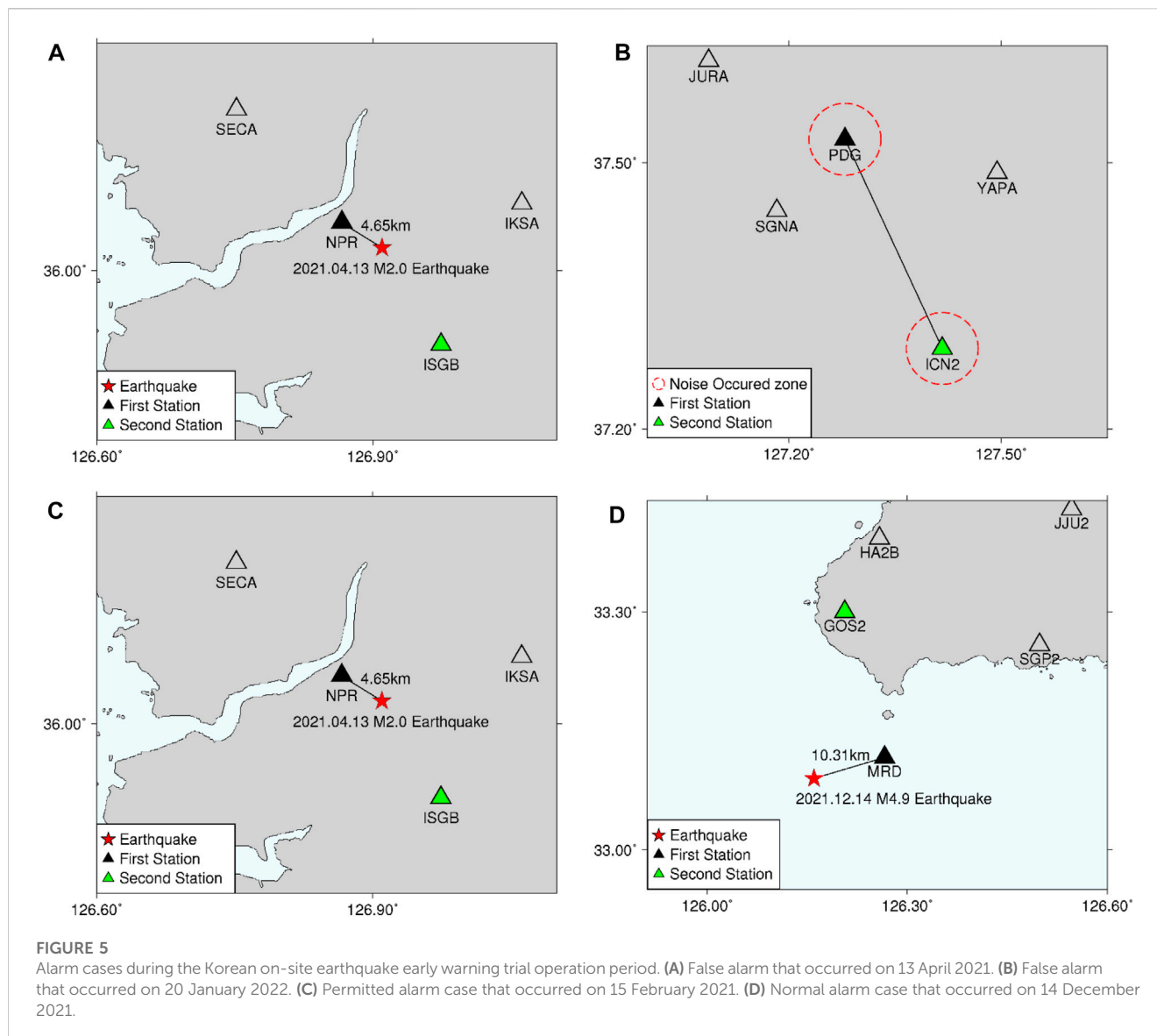
Table 4 includes the initial report time and the first detected station information for network-based EEW. The initial report time is the time when seismic source information is generated based on three or more detection stations. However, the information

TABLE 4 List of earthquakes used for test operation ($M_L \geq 2.0$).

No.	Origin time (UTC)	Latitude (°)	Longitude (°)	M_L	Depth (km)	IM	FDAS			Network-based EEW 1st report time (s)
							Name	Epicentral distance (km)	Detected time (s)	
1	11-06-2020 09:27:23	36.43	128.14	2.0	8	II	SAJB	2.91	+2	+7
2	11-08-2020 06:26:09	36.41	128.22	2.9	9	IV	SAJB	5.60	+2	+6
3	11-14-2020 15:00:29	35.76	129.18	2.1	17	III	DUC	1.76	+3	+5
4	12-23-2020 12:28:20	37.73	126.73	2.2	12	III	GMPB	10.88	+3	+6
5	02-05-2021 19:40:03	35.81	127.53	2.7	5	IV	DGHA	4.65	+2	+6
6	02-15-2021 09:59:25	35.99	126.84	2.5	14	IV	NPR	6.30	+3	+7
7	03-15-2021 17:51:52	35.76	129.19	2.6	18	III	DUC	2.15	+2	+6
8	04-13-2021 12:56:15	36.02	126.91	2.0	13	III	NPR	4.65	+2	+6
9	04-19-2021 05:20:27	35.07	125.08	3.7	15	II	HGDB	41.87	+8	+16
10	05-12-2021 21:04:28	35.89	127.33	2.0	10	III	JEO2	6.29	+3	+7
11	07-30-2021 20:17:10	35.65	128.4	2.5	22	III	CHRB	14.67	+4	+7
12	08-29-2021 04:03:23	35.31	128.49	2.2	9	III	CLSA	5.87	+2	+7
13	09-11-2021 17:04:46	35.53	128.53	2.1	13	II	CHPR	4.75	+2	+6
14	09-19-2021 21:58:49	34.88	127.25	2.2	8	III	MNDB	12.59	+2	+6
15	09-23-2021 03:02:43	35.42	128.49	2.6	16	IV	CLSA	6.36	+2	+7
16	10-06-2021 12:55:48	35.25	127.86	2.5	13	III	SACA	18.22	+4	+7
17	11-11-2021 16:31:05	36.15	129.38	2.1	8	II	PHA2	4.85	+2	+6
18	12-14-2021 08:19:14	33.09	126.16	4.9	17	V	MRD	10.30	+4	+13 (Alert: +16)
19	12-15-2021 13:02:14	35.79	127.8	2.3	10	IV	WICA	6.54	+3	+8
20	01-21-2022 16:08:37	32.73	132.10	6.7	31	III	BSAA	381.37		Out layer
21	02-02-2022 03:04:55	35.72	128.99	2.4	19	III	GSNA	4.59	+4	+8
22	03-05-2022 13:16:21	36.39	127.13	2.4	12	III	KOJ2	9.08	+3	+8

generated at this time may not be completely reliable (Cho et al., 2022b). Therefore, the KMA takes into account decision-making factors for notification judgments. There was one actual alarm, which was the earthquake that occurred in the Seogwipo sea area on 14 December 2021, with a M_L 4.9. The alert of EEW were issued for this event as it was predicted to be M_L 5.3 (No. 18 event).

FIGURE 5
Alarm cases during the Korean on-site earthquake early warning trial operation period. **(A)** False alarm that occurred on 13 April 2021. **(B)** False alarm that occurred on 20 January 2022. **(C)** Permitted alarm case that occurred on 15 February 2021. **(D)** Normal alarm case that occurred on 14 December 2021.

4 Results and discussion

4.1 Warning cases during the trial operation

The EEW alarm can be classified as 'normal' if they correctly detect an earthquake, 'miss' if they fail to detect an earthquake, and 'false' if they report an earthquake when none has occurred. Non-seismic events (e.g., artificial signal, ambient noise) or micro-earthquakes were classified as false alarms and normal operations. During the trial operation, no alarm failure cases occurred. Among the total of 22 earthquakes that occurred, four raised alarms. An earthquake case issued an accurate warning according to the threshold set in the system. Two additional warnings that did not meet the threshold and one warning due to a non-earthquake were also issued, confirming the cases of false alarms. In the rest of the event cases, no alarms were generated because the seismic waves did not exceed the set threshold. Therefore, it was considered normal operation.

The two false alarm cases were thoroughly reviewed. The first case in Figure 5A is an earthquake that occurred on 13 April 2021. Here, the predicted IM was higher than the seismic intensity announced by the KMA. Three seconds after the earthquake, a signal was detected at the NPR station, 4.65 km away from the epicenter. The initial P-wave caused by the earthquake was accurately identified. Next, the P-wave was detected at the second station (ISGB). Figure 6A shows the waveforms recorded at each station. Although the earthquake was detected at the second station, the IM was predicted as V, based on the amplitude of the initial P-wave recorded at the first station; an alarm was triggered immediately. However, the observed MMI was III, for which no alert should have been issued.

In the second false alarm case (see Figure 5B), signals were simultaneously detected at the PDG and ICN2 stations on 20 January 2022. The seismic intensity and magnitude could not be recorded because it was not an earthquake. However, the Step
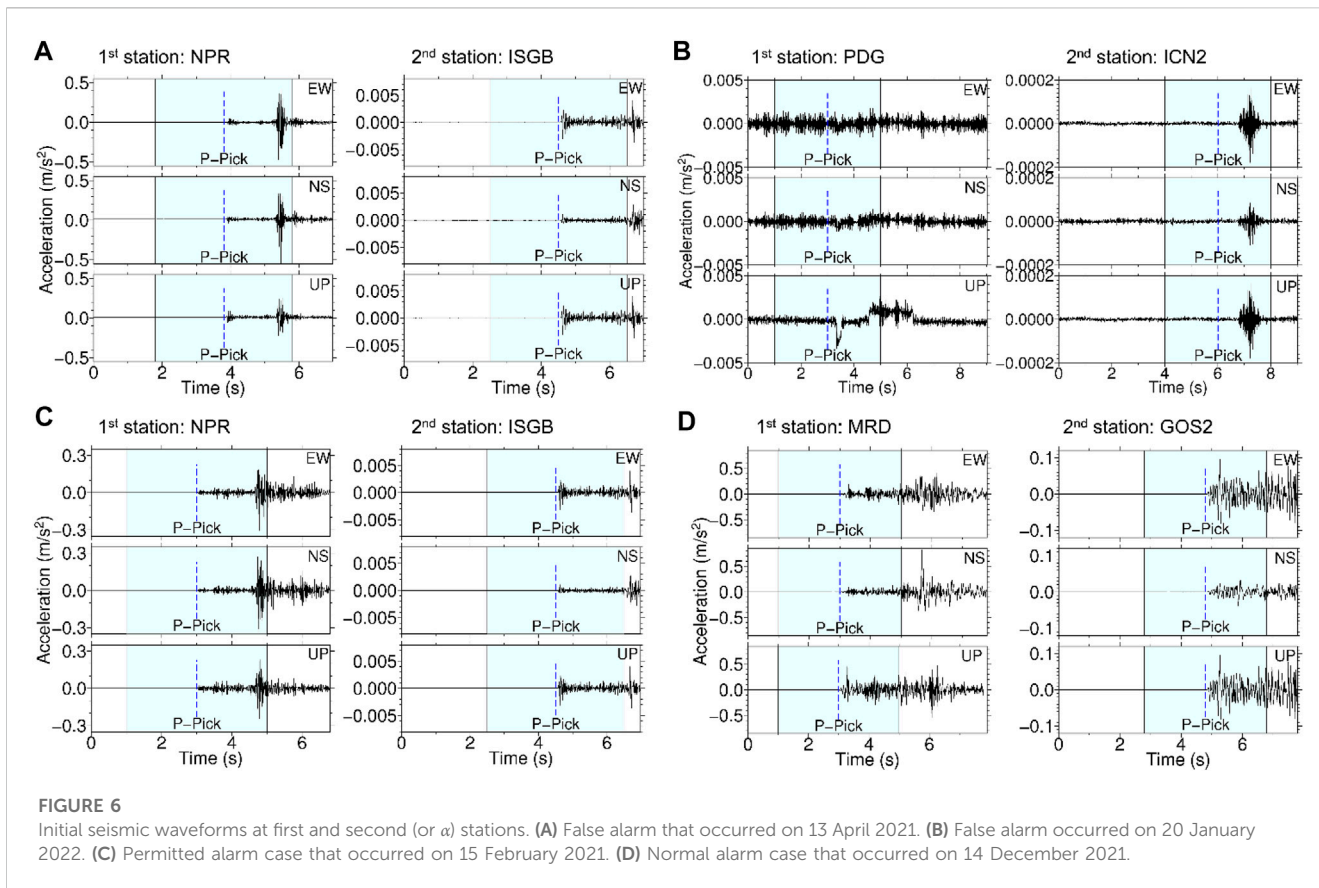
FIGURE 6
Initial seismic waveforms at first and second (or α) stations. **(A)** False alarm that occurred on 13 April 2021. **(B)** False alarm occurred on 20 January 2022. **(C)** Permitted alarm case that occurred on 15 February 2021. **(D)** Normal alarm case that occurred on 14 December 2021.

TABLE 5 Classification of alarm types based on confusion matrix.

Section		KOS EEW[a] operation (or prediction)	
		Warning	No warning
Signal	Moderate–large earthquake (*IM* at the first detection station ≥ V)	Normal/permitted alarm (*TP*[b])	Missed alarm (*FN*[c])
	Small earthquake (*IM* at the first detection station < V) or Non-seismic event	False alarm (*FP*[d])	Normal operation (*TN*[e])

[a]KOS EEW: Korean on-site earthquake early warning.
[b]*TP*: true positive.
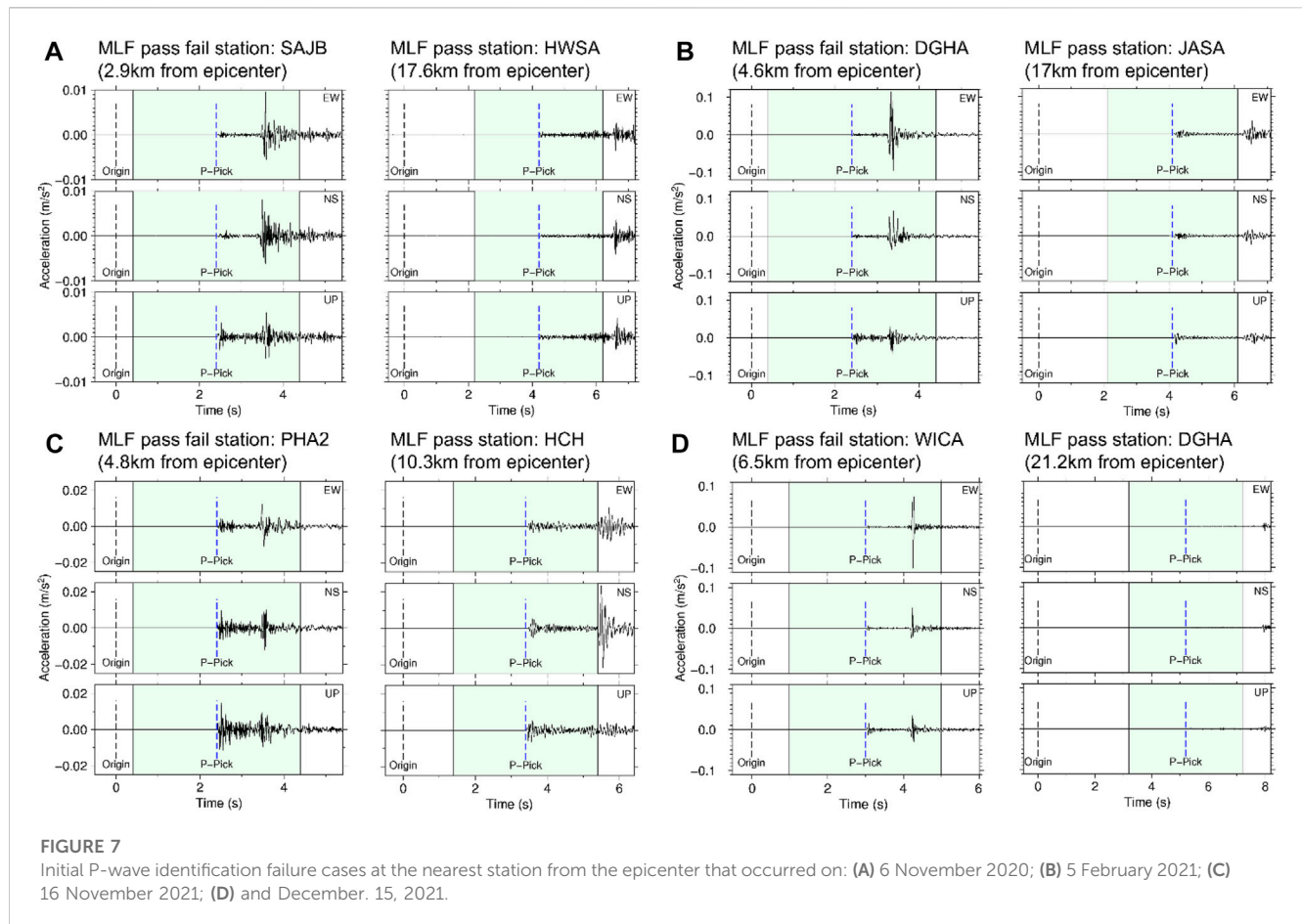[c]*FN*: false negative.
[d]*FP*: false positive.
[e]*TN*: true negative.

TABLE 6 Results of the confusion matrix of Korean on-site earthquake early warning (KOS EEW) system.

Section		KOS EEW without step 4		KOS EEW	
		Warning	No warning	Warning	No warning
Signal	Moderate–large earthquake (*IM* at the first detection station ≥ V)	2	0	2	0
	Small earthquake (*IM* at the first detection station < V) or Non-seismic event	29	1,190,529	2	1,190,556

2 filter identified a signal as a P-wave at the first station. The predicted IM was V, and subsequently the signal was detected at the ICN2 station, which was 28.88 km away from the first one. The signals recorded at both stations are shown in Figure 6B. The two signals did not have similar amplitude over time and showed different frequency components. Thus, it was hypothesized that they were generated by two unrelated sources that did not correlate with each other. It was confirmed that temporary noise generated at

FIGURE 7
Initial P-wave identification failure cases at the nearest station from the epicenter that occurred on: **(A)** 6 November 2020; **(B)** 5 February 2021; **(C)** 16 November 2021; **(D)** and December. 15, 2021.

two nearby stations could be misinterpreted as an event, resulting in a false alarm.

The permitted alarm case is shown in Figure 5C. An earthquake of M_L 2.5 occurred on 15 February 2021. The OFPK detected the signal at the NPR station located 6.3 km from the epicenter, 3.7 s after the earthquake. A permitted warning was determined as the signal was subsequently detected at the nearby ISGB station. Furthermore, the observed seismic intensity was IV, which differed from the predicted value and did not exceed the warning threshold. Therefore, the issued alarm was acceptable because there was a possibility of vibration being felt at the stations closest to the epicenter. Waveform records are shown in Figure 6C. In KOS EEW, the NPR station overestimated IM and issued alarms twice during the trial. In Figure 6, specific cases in which the S-wave reached within 2 s of the P-wave time window (PTW) were shown and the S-wave in the PTW-induced overestimation MMI in Step 3 was included.

The second is a normal alarm case caused by an earthquake of M_L 4.9 that occurred in the Seogwipo sea area on 14 December 2021. This case is shown as Figure 5D. It was the eighth most severe earthquake to strike the Korean Peninsula since digital seismic observation began in 1999, causing significant seismic vibration at the site. The network-based EEW calculated the magnitude as 5.3 in the initial analysis using records from eight observation stations. Accordingly, an early warning was issued via text

messages on Jeju Island. For this case, the KOS EEW analysis was as follows. A signal was detected at the MRD station, 10.31 km away from the epicenter, 4.1 s after the earthquake, and passed the P-wave identification stage. The predicted IM at the MRD station passed the warning threshold as VI and a normal warning was determined immediately after the signal was detected at the nearby GOS2 station. The results are shown in Figure 6D.

4.2 KOS EEW performance evaluation for warning decision

To determine the performance of the on-site EEW, four types of events were examined using the confusion matrix that allows the analysis of Type 1 and Type 2 errors. The different types of alarms for the base of the confusion matrix are summarized in Table 5. Earthquake alarms issued are classified as normal and missed alarms, and if no alerts are required, they are classified as false alarms and normal operation. As an exception, if KOS EEW determined an alarm of an event in which the specific station recorded a seismic intensity of IV, it was regarded as an accepted (or permitted) operation. This case occasionally occurs in Step 3 (the IM prediction Step). In Step 3, the empirical function based on linear regression analysis was applied in KOS EEW. If the difference between the predicted and observed intensities is one or less, it is
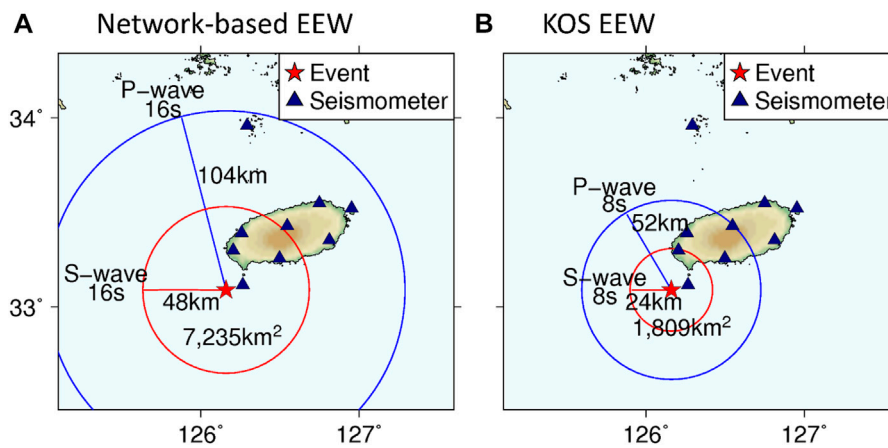
FIGURE 8
Blind zone for the 12.14.2021 ML4.9 earthquake. **(A)** The case of network-based earthquake early warning (EEW) and **(B)** the case of KOS EEW. The blue and dashed lines are the distance and radius that the P-wave can travel in 16 s. The red and dashed lines are the distance and radius that the S-wave can travel in 16 s. S-wave radius at the time of alarm decision is the blind zone.
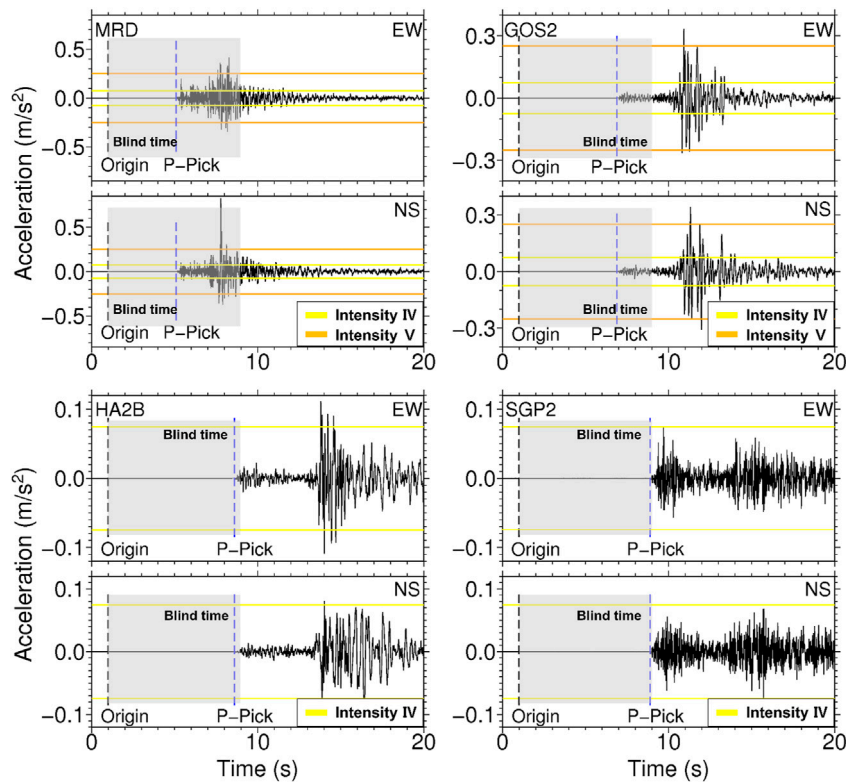

FIGURE 9
Lead times for seismic stations based on intensity measurements. Blind time is the interval zone before the alarm of KOS EEW, and it is illustrated in a gray box.

considered an acceptable level of error. Therefore, it was defined as a permitted alarm and classified as a normal alarm. In the confusion matrix, normal and permissible alarms belong to true positive (*TP*), false alarms belong to false positive (*FP*), and normal operations belong to true negative (*TN*). Missed alarms belong to false negative (*FN*); however, they did not occur during the trial operation.

TABLE 7 Comparison of lead time.

Station name	Epicentral distance (km)	RPT[a] (s)	NWT[b] − RPT (s)	KWT[c] − RPT (s)	KWT[c] − E4T[d] (s)	KWT[c] − E5T[e] (s)
MRD	10.30	6.8	- 9.2	- 1.2	- 3.5	−1.4
GOS2	23.72	10.3	- 5.7	2.3	1.7	2.7
HA2B	34.85	13.0	- 3.0	5.0	4.8	-
SGP2	36.59	14.7	- 1.3	6.7	0.8	-
JJU2	52.10	18.6	2.6	10.6	-	-
PYSB	67.46	23.2	7.2	15.2	-	-
GUJA	74.98	27.7	11.7	19.7	-	-
UDO	88.09	31.3	15.3	23.3	-	-
CJD	97.46	32.2	16.2	24.2	-	-

[a]RPT: Record time of PGA.
[b]NWT: warning time of Network-based EEW (= Origin time +16 s).
[c]KWT: warning time of KOS EEW (= Origin time +8 s).
[d]E4T: Excess time of IV.
[e]E5T: Excess time of V.

The performance of the model by setting different criteria was additionally evaluated. The social responsibility of public institutions that issue disaster alerts may be more important than situations induced by errors or false alarms. False alarms in EEW systems have caused panic and confusion in the past. For example, in Japan, a false alarm in January 2018 mistakenly recognized two small earthquakes as one big earthquake, leading to temporary panic among millions of people. The head of the Japan Meteorological Administration had to apologize for the mistake (BBC, 2018). Similarly, in the United States, a warning about a large-scale earthquake off the coast of California was issued 92 years after it had actually occurred due to a computer error, causing confusion among people (BBC, 2017). In Mexico, a false alert was issued in July 2014 by Sky Alert, a popular smartphone app, resulting in many people responding to the false alarms (Reddy, 2020). These incidents highlighted the importance of effective management in ensuring the reliability and effectiveness of such system.

Based on the confusion matrix, the performance evaluation was classified into two categories: 1) KOS EEW and 2) KOS EEW without Step 4. KOS EEW without Step 4 is a non-applied 1+ α station method. Both methods are summarized in Table 6.

The P-waves that exceed the alarm threshold were assigned to "Positive" class, and the S-wave and noise signal of microearthquakes were classified as "Negative" class for 1,190,560 sample data that occurred in 2021. KOS EEW without Step 4 produced more alarms than KOS EEW, and it was confirmed that 27 additional alarms could be triggered. Accuracy is defined as the number of correct precedents (i.e., TP and TN) divided by the number of cases (TP, TN, FP, FN) that can be caused by KOS log data Eq. 10. In both cases, the accuracy was close to 100% because numerous non-alarm signals occurred during the test operation. Therefore, the primary focus was on the cases where an alarm occurred (TP and FP). The precision was calculated as the number of normal and permitted alarms (TP) divided by the total number of warnings (sum of TP and FP) Eq. 11. Precision was 6.4% and 50% for KOS EEW without Step 4 and KOS EEW, respectively. Therefore, KOS EEW

determines alarms with a higher precision capability than KOS EEW without Step 4.

$$Accuracy = \frac{TP + TN}{TP + FP + TN + FN} \qquad (10)$$

$$Precision = \frac{TP}{TP + FP} \qquad (11)$$

In addition, a few cases of failed analysis were found at the first station, during the trial operation for small earthquakes finally determined as normal operations. Out of 22 analyzed events, P-wave identification failed in four earthquakes at the first station (refer to Figure 7). Although the analysis using waveforms at the first station failed, the signals at the respective second stations were classified as P-wave and passed Step 2. Such failures did not cause problems in the warning process, as they were finally determined to be normal operation without alarms for small magnitude events. The picking time and MLF passes by each station for the four earthquakes are summarized in Supplementary Appendix S1. The picking times for the two stations required for the KOS EEW were 5.1, 4.2, 3.4, and 5.2 s after the earthquake occurred. The picking times required for the network-based EEW were 5.8, 5.6, 4.6, and 5.7 s. Therefore, even if P-wave identification fails at the first station, KOS EEW can notify an earthquake faster than the network-based EEW. This method makes our seismic warning system more stable by additional filtering, and the output results mis-analyzed in the previous step are not passed to the next step. However, a reinforcement cement method may be necessary, including Step 2 of MLF.

4.3 Comparison of network-based EEW and KOS EEW

The potential effectiveness of an EEW system based on the lead time and blind zone could be estimated. In the case of the Seogwipo sea area event (14 December 2021, M_L 4.9) on Jeju Island, the network-based EEW in the KMA estimated a magnitude of 5.3 based on eight stations, and Jeju citizens
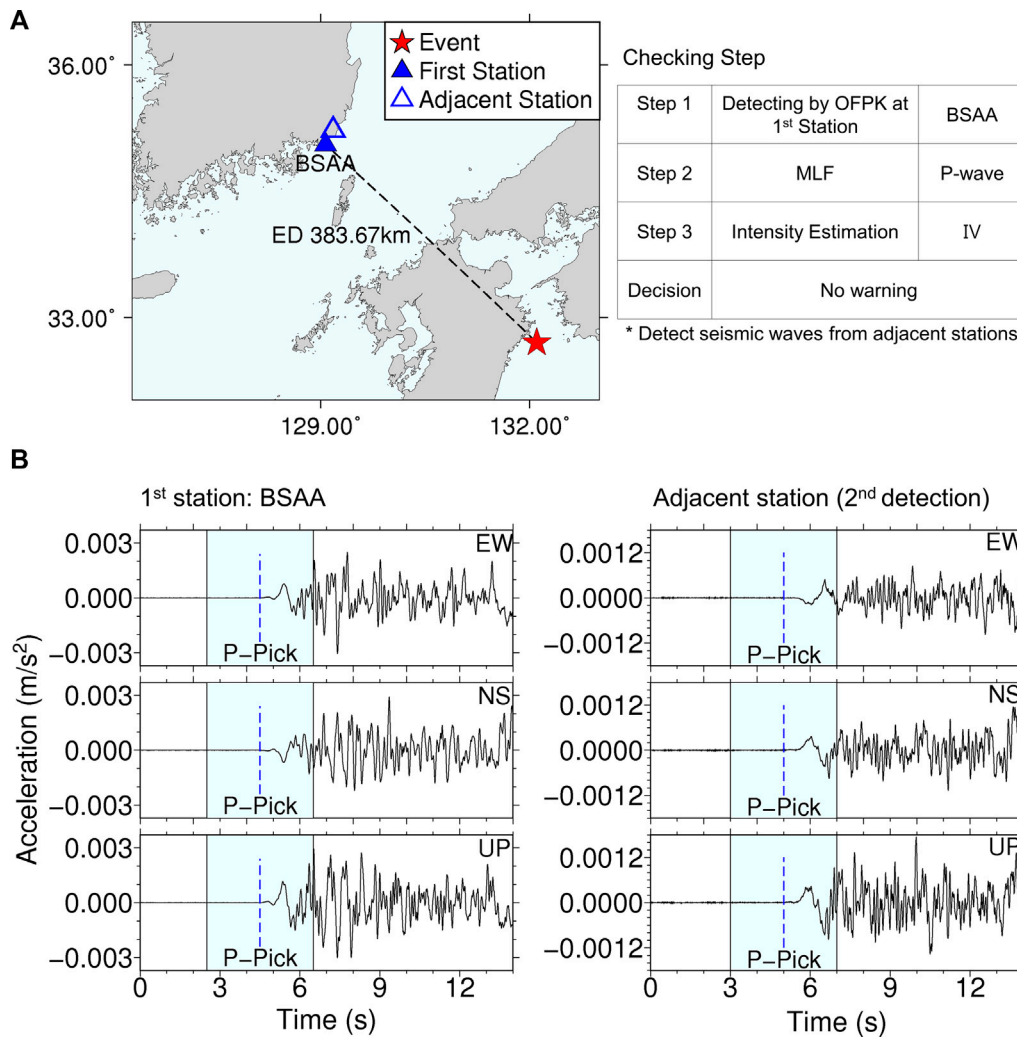
FIGURE 10
Application of the KOS EEW outside the Korean seismic network. Case of an earthquake (Table 4, No. 20) outside the KMA seismic network: **(A)** Epicenter and detected stations **(B)** Seismic waveform at the detected stations.

received the message through the cell broadcasting service, because the magnitude of 5.3 of network-based EEW was estimated with the initial P-wave for eight trigger data. However, a reanalysis of source parameters showed that the magnitude was less than that calculated by EEW. The KMA confirmed this earthquake 13 s after it occurred (Table 4, No, 18). In the case of a sea earthquake, determining the location with only the three observations is difficult, and additional observation stations are needed to calculate the location and magnitude. As a result, Jeju citizens received an earthquake early warning message 16 s after the earthquake occurred. At this time, the added time of 3 s due to the communication propagation time. In contrast, in KOS EEW, the entire process of issuing the on-site alarm would take only 8 s, including the telecommunication transmission time. The blind zone area was estimated based on the time to send the alarm (see Figure 8). The propagation speeds of the P- and S-waves were assumed to be 6.5 and 3 km/s, respectively. KOS EEW reduced the blind zone by one-fourth compared to the 7,235 km² of the network-based EEW.

The lead time based on the seismic observatories on Jeju Island was analyzed. The delivery of alert time in both network-based EEW and on-site EEW was defined in the same way as the blind zone. The times between the warnings and the arrival of shaking are variable according to the area or platform (McBride et al., 2023). However, it was assumed that the communication delay time was to be 3s. Most users trained in earthquake response can react to drop, cover, and hold on (DCHO) after an early warning message (Porter, 2016). Users who receive an EEW require 3s to follow the DCHO protocol (Minson et al., 2018). Therefore, the minimum lead time of 3s was applied.

Figure 9 presents the results of the lead time analysis for each seismic station based on the improved MMI. The MMI criterion set by KOS is V, but for closer examination, we also set it to IV. The exact lead times based on the threshold of IV are summarized in Table 7. For seismic structural engineering applications of EEW, the strategy of threshold-based IM can be adopted (Iervolino, 2011). When the lead time is based on PGA, the network-based

EEW can prepare for any damage induced by earthquake at GOS2 station. However, if the lead time is determined based on PGA in areas near the epicenter, it is likely to be set as a time after damage. Therefore, it is required to standardize for vibrations of induced damage rather than the reference based on IM. When setting the threshold of IV, the lead time was decreased at the MRD, GOS2, and HA2B observatories. Consequently, KOS EEW shows it could prevent damage from 34.85 km (based on the HA2B station).

In addition, teleseismic earthquakes that occurred during the trial operation period were analyzed. On 21 January 2022, at 16:08:37 (UTC), an earthquake of M_L 6.7 occurred 73 km southeast of Oita Prefecture, Japan (see Figure 10). The maximum seismic intensity III was recorded in Busan and the observed seismic intensity in the surrounding area was II. In the KOS EEW, a signal was detected at BSAA, approximately 834 km from the epicenter, 88.5 s after the earthquake occurrence. The signal was identified as a P-wave in Step 2 MLF. However, the predicted MMI did not pass the threshold. Therefore, it was classified as a normal operation.

This confirmed the potential of the KOS EEW response to large teleseismic earthquakes, although the advantage of on-site EEW in reducing the blind zone cannot be confirmed. The KOS EEW could generate alarms for the teleseismic events if the IM exceeded the warning thresholds. The potential of the KOS EEW to generate an alarm using data from local stations for large earthquakes in nearby countries, such as Japan or China, was displayed.

5 Conclusion

This study reviewed the effectiveness of the on-site EEW system to prepare for earthquake disasters in urban cities or social infrastructure and thoroughly summarized MLF and outfitting models. Subsequently, a real-time trial operation of KOS EEW was carried out to evaluate and verify its stable alert decisions and performance, and the following conclusions can be drawn.

(1) In order to develop KOS EEW, empirical methods were combined with robust methods based on artificial intelligence. This process was able to effectively avoid overfitting and improve P-wave detection. The proposed MLF procedure increased the success rate of P-wave detection; however, it was not perfect. Therefore, connection of a second station was used for filtering out false positives belonging to non-seismic events called the $1+ \alpha$ method, which was effective when the spatial density of the observation stations was secured to cover the high-frequency vibration damping effect.

(2) We conducted a test-run of a KOS EEW that utilizes fewer observatories than the network EEW, and confirmed its effectiveness in providing prompt notifications during the Seogwipo Sea area earthquake event. This method also showed a reduction of more than a quarter in the blind zone. However, to fully utilize KOS EEW for Management Perspective, it is still wondering to determine the optimal alarm method and control the rate of false alarms.

(3) The network-based EEW can provide accurate earthquake information and stable warning to the public. On the other hand, KOS EEW prioritizes speed and may not provide comprehensive information about earthquakes to citizens. In terms of damage prevention, KOS EEW has set a standard IM, and warnings are triggered when there is strong vibration in the target area of the earthquake. Therefore, this technology is expected highly utilizable to reduce earthquake damage based on trial test cases.

(4) Korea's seismic observation network is undergoing changes to enhance earthquake observation and EEW (Cho et al., 2022a). As a result, borehole-type seismometers are being installed more frequently than on the ground surface, which is different from other countries. Consequently, methods predicting intensity measures based on boreholes are being developed (Jang et al., 2023; Lim and Ahn, 2023). However, due to the lack of data from the changed observation network, it is challenging to improve P-wave detection accuracy. In the future, MLF's P-wave detection accuracy will need to be improved through additional earthquake data training, and prediction accuracy can be further enhanced by considering site effects.

Data availability statement

The original contributions presented in the study are included in the article, further inquiries can be directed to the corresponding author.

Author contributions

J-KA: Supervision, Original Draft, Conceptualization, Writing, Data design and Analysis; EP: Original Draft, Data processing and Analysis; BK: Writing, Original Draft and Machine Learning Analysis; E-HH: EEW expertise and Supervision; SH: Writing and Supervision. All authors have read and agreed to the published version of the manuscript.

Funding

Acknowledgments

Conflict of interest

The authors declare that the research was conducted in the absence of any commercial or financial relationships that could be construed as a potential conflict of interest.

Publisher's note

All claims expressed in this article are solely those of the authors and do not necessarily represent those of their affiliated organizations, or those of the publisher, the editors and the reviewers. Any product that may be evaluated in this article, or claim that may be made by its manufacturer, is not guaranteed or endorsed by the publisher.

Supplementary material

The Supplementary Material for this article can be found online at: https://www.frontiersin.org/articles/10.3389/feart.2023.1157742/full#supplementary-material

References

Allen, R. M. (1982). Automatic phase pickers: Their present use and future prospects. *Bull. Seismol. Soc. Amer.* 72, S225–S242. doi:10.1785/bssa07206b0225

Allen, R. M., and Melgar, D. (2019). Earthquake early warning: Advances, scientific challenges, and societal needs. *Annu. Rev. Earth. Planet. Sci.* 47, 361–388. doi:10.1146/annurev-earth-053018-060457

Aminpour, M., Alaie, R., Khosravi, S., Kardani, N., Moridpour, S., and Nazem, M. (2023). Slope stability machine learning predictions on spatially variable random fields with and without factor of safety calculations. *Comput. Geotech.* 153, 105094. doi:10.1016/j.compgeo.2022.105094

BBC (2017). California earthquake alarm sounded - 92 years late. Available at: https://www.bbc.com/news/technology-40366816.

BBC (2018). False earthquake warning panics Japan. Available at: https://www.bbc.com/news/world-asia-42582113.

Becker, J. S., Potter, S. H., Vinnell, L. J., Nakayachi, K., McBride, S. K., and Johnston, D. M. (2020). Earthquake early warning in aotearoa New Zealand: A survey of public perspectives to guide warning system development. *Humanit. Soc. Sci. Commun.* 7, 138. doi:10.1057/s41599-020-00613-9

Behr, Y., Clinton, J. F., Cauzzi, C., Hauksson, E., Jónsdóttir, K., Marius, C. G., et al. (2016). The virtual seismologist in SeisComP3: A new implementation strategy for earthquake early warning algorithms. *Seismol. Res. Lett.* 87, 363–373. doi:10.1785/0220150235

Bindi, D., Iervolino, I., and Parolai, S. (2016). On-site structure-specific real-time risk assessment: Perspectives from the REAKT project. *Bull. Seismol. Soc. Am.* 14, 2471–2493. doi:10.1007/s10518-016-9889-4

Bossu, R., Finazzi, F., Steed, R., Fallou, L., and Bond, I. (2022). Shaking in 5 seconds!" - performance and user appreciation assessment of the earthquake network smartphone-based public earthquake early warning system. *Seismol. Res. Lett.* 93, 137–148. doi:10.1785/0220210180

Bostrom, A., McBride, S. K., Becker, J. S., Goltz, J. D., de Groot, R. M., Peek, L., et al. (2022). Great expectations for earthquake early warnings on the United States West Coast. *Int. J. Disaster Risk Reduc.* 82, 103296. doi:10.1016/j.ijdrr.2022.103296

Caruso, A., Colombelli, S., Elia, L., Picozzi, M., and Zollo, A. (2017). An on-site alert level early warning system for Italy. *J. Geophys. Res. Solid Earth.* 122, 2106–2118. doi:10.1002/2016JB013403

Chen, D. Y., Hsiao, N. C., and Wu, Y. M. (2015). The Earthworm based earthquake alarm reporting system in Taiwan. *Bull. Seismol. Soc. Am.* 105, 568–579. doi:10.1785/0120140147

Cho, S., Ahn, J. K., and Hwang, E. H. (2022b). Optimization of network-based earthquake early warning systems on the Korean Peninsula. *IEEE Access* 10, 83931–83939. doi:10.1109/ACCESS.2022.3197661

Cho, S., Lee, M. G., Ahn, J. K., Sun, C. G., and Kim, H. S. (2022a). Site flatfile of Korea meteorological administration's seismic stations in Korea. *Bull. Earthq. Eng.* 20, 5775–5795. doi:10.1007/s10518-022-01418-8

Chung, A. I., Henson, I., and Allen, R. M. (2019). Optimizing earthquake early warning performance: ElarmS-3. *Seismol. Res. Lett.* 90, 727–743. doi:10.1785/0220180192

Colombelli, S., Caruso, A., Zollo, A., Festa, G., and Kanamori, H. A. (2015). A P wave-based, on-site method for earthquake early warning. *Geophys. Res. Lett.* 42, 1390–1398. doi:10.1002/2014GL063002

Cremen, G., and Galasso, C. (2020). Earthquake early warning: Recent advances and perspectives. *Earth. Sci. Rev.* 205, 103184. doi:10.1016/j.earscirev.2020.103184

Dallo, I., Marti, M., Clinton, J., Böse, M., Massin, F., and Zaugg, S. (2022). Earthquake early warning in countries where damaging earthquakes only occur every 50 to 150 years–The societal perspective. *Int. J. Disaster Risk Reduc.* 83, 103441. doi:10.1016/j.ijdrr.2022.103441

Datta, A., Wu, D. J., Zhu, W., Cai, M., and Ellsworth, W. L. (2022). DeepShake: Shaking intensity prediction using deep spatiotemporal RNNs for earthquake early warning. *Seismol. Soc. Am.* 93, 1636–1649. doi:10.1785/0220210141

Doi, K. (2011). The operation and performance of earthquake early warnings by the Japan Meteorological Agency. *Soil. Dyn. Earthq. Eng.* 31, 119–126. doi:10.1016/j.soildyn.2010.06.009

Eichenberger, J., Ferrari, A., and Laloui, L. (2013). Early warning thresholds for partially saturated slopes in volcanic ashes. *Comput. Geotech.* 49, 79–89. doi:10.1016/j.compgeo.2012.11.002

Fujinawa, Y., and Noda, Y. (2013). Japan's earthquake early warning system on 11 March 2011: Performance, shortcomings, and changes. *Earthq. Spectra.* 29, 341–368. doi:10.1193/1.4000127

He, X., Xu, H., Sabetamal, H., and Sheng, D. (2020). Machine learning aided stochastic reliability analysis of spatially variable slopes. *Comput. Geotech.* 126, 103711. doi:10.1016/j.compgeo.2020.103711

Heaton, T. H. (1985). A model for a seismic computerized alert network. *Science* 228, 987–990. doi:10.1126/science.228.4702.987

Hsiao, N. C., Wu, Y. M., Shin, T. C., Zhao, L., and Teng, T. L. (2009). Development of earthquake early warning system in Taiwan. *Geophys. Res. Lett.* 2, L00B02. doi:10.1029/2008GL036596

Iervolino, I. (2011). Performance-based earthquake early warning. *Soil Dyn. Earthq. Eng.* 31, 209–222. doi:10.1016/j.soildyn.2010.07.010

Jang, D., Ahn, J. K., Kim, T. W., and Kwak, D. Y. (2023). Linearly combined ground motion model using quadratic programming for low-to mid-size seismicity region: South Korea. *Front. Earth Sci.* 10, 1067802. doi:10.3389/feart.2022.1067802

Kanamori, H. (2005). Real-time seismology and earthquake damage mitigation. *Annu. Rev. Earth. Planet. Sci.* 33, 195–214. doi:10.1146/annurev.earth.33.092203.122626

Korea Meteorological Administration (2022). Technology development of application and support for the earthquake and volcanic service (Ⅵ): Optimization of earthquake detection algorithm for onsite warning. Report No. 11-1360000-001781-10.

Lee, H., Jeon, I., Seo, J., and Lee, J. (2020). Application of the onsite EEW technology using the P-wave of seismic records in Korea. *J. Soc. Disaster Inf.* 16, 133–143. doi:10.10683/KOSDI.2020.3.31.133

Lee, H. (2020). On-site alarm technical and applied research for earthquake regions. R&D No KMI2018-02210. doi:10.23000/TRKO202200009916

Lim, D., and Ahn, J. K. (2023). Horizontal seismic wave at ground surface from transfer function based on ambient noise. *Front. Earth Sci.* 11, 1047667. doi:10.3389/feart.2023.1047667

Liu, Q., Jian, W., and Nie, W. (2021). Rainstorm-induced landslides early warning system in mountainous cities based on groundwater level change fast prediction. *Sustain. Cities. Soc.* 69, 102817. doi:10.1016/j.scs.2021.102817

Lomax, A., Satriano, C., and Vassallo, M. (2012). Automatic picker developments and optimization: FilterPicker—a robust, broadband picker for real-time seismic monitoring and earthquake early warning. *Seismol. Res. Lett.* 83, 531–540. doi:10.1785/gssrl.83.3.531

McBride, S. K., Sumy, D. F., Llenos, A. L., Parker, G. A., McGuire, J., Saunders, J. K., et al. (2023). Latency and geofence testing of wireless emergency alerts intended for the ShakeAlert® earthquake early warning system for the West Coast of the United States of America. *Saf. Sci.* 157, 105898. doi:10.1016/j.ssci.2022.105898

Meier, M. A., Ross, Z. E., Ramachandran, A., Balakrishna, A., Nair, S., Kundzicz, P., et al. (2019). Reliable real-time seismic signal/noise discrimination with machine learning. *J. Geophys. Res. Solid Earth.* 124, 788–800. doi:10.1029/2018JB016661

Minson, S. E., Meier, M. A., Baltay, A. S., Hanks, T. C., and Cochran, E. S. (2018). The limits of earthquake early warning: Timeliness of ground motion estimates. *Sci. Adv.* 4, eaaq0504. doi:10.1126/sciadv.aaq0504

Mittal, H., Wu, Y. M., Sharma, M. L., Yang, B. M., and Gupta, S. (2019). Testing the performance of earthquake early warning system in northern India. *Acta. Geophys.* 67, 59–75. doi:10.1007/s11600-018-0210-6

Mousavi, S. M., Ellsworth, W. L., Zhu, W., Chuang, L. Y., and Beroza, G. C. (2020). Earthquake transformer-an attentive deep-learning model for simultaneous earthquake detection and phase picking. *Nat. Commun.* 11, 3952–4012. doi:10.1038/s41467-020-17591-w

Mousavi, S. M., Zhu, W., Sheng, Y., and Beroza, G. C. (2019). Cred: A deep residual network of convolutional and recurrent units for earthquake signal detection. *Sci. Rep.* 9, 10267–10314. doi:10.1038/s41598-019-45748-1

Nakamura, Y. (1988). "On the urgent earthquake detection and alarm system (UrEDAS)," in Proc. of the 9th World Conference on Earthquake Engineering in Tokyo-Kyoto, 2-9 August 1988 (Berlin, Germany: Springer), 249–281. doi:10.1007/978-3-540-72241-0_13

Nakamura, Y., Saita, J., and Sato, T. (2011). On an earthquake early warning system (EEW) and its applications. *Soil. Dyn. Earthq. Eng.* 31, 127–136. doi:10.1016/j.soildyn.2010.04.012

Nakamura, Y., and Saita, J. (2007). "UrEDAS, the earthquake warning system: Today and tomorrow," in *Earthquake early warning systems* (Berlin, Heidelberg: Springer), 249–281.

Nakayachi, K., Becker, J. S., Potter, S. H., and Dixon, M. (2019). Residents' reactions to earthquake early warnings in Japan. *Risk Anal.* 39, 1723–1740. doi:10.1111/risa.13306

National Academies of Sciences (2018). *Engineering, and medicine emergency alert and warning systems: Current knowledge and future research directions.* Washington, DC: The National Academies Press. doi:10.17226/24935

Ozsagir, M., Erden, C., Bol, E., Sert, S., and Özocak, A. (2022). Machine learning approaches for prediction of fine-grained soils liquefaction. *Comput. Geotech.* 152, 105014. doi:10.1016/j.compgeo.2022.105014

Parolai, S., Bindi, D., Boxberger, T., Milkereit, C., Fleming, K., and Pittore, M. (2015). On-site early warning and rapid damage forecasting using single stations: Outcomes from the REAKT project. *Seismol. Res. Lett.* 86, 1393–1404. doi:10.1785/0220140205

Parolai, S., Oth, A., and Boxberger, T. (2017). Performance of the GFZ decentralized on-site earthquake early warning software (GFZ-sentry): Application to K-NET and KiK-net recordings, Japan. *Seismol. Res. Lett.* 88, 1480–1490. doi:10.1785/0220170048

Picozzi, M., Zollo, A., Brondi, P., Colombelli, S., Elia, L., and Martino, C. (2015). Exploring the feasibility of a nationwide earthquake early warning system in Italy. *J. Geophys. Res. Solid Earth.* 120 (4), 2446–2465. doi:10.1002/2014JB011669

Porter, K. A. (2016). *How many injuries can be avoided through earthquake early warning and drop, cover, and hold on?* Boulder, CO: Structural Engineering and Structural Mechanics Program.

Reddy, E. (2020). Crying 'crying wolf': How misfires and Mexican engineering expertise are made meaningful. *Ethnos* 85, 335–350. doi:10.1080/00141844.2018.1561489

Santos-Reyes, J. (2019). How useful are earthquake early warnings? The case of the 2017 earthquakes in Mexico city. *Int. J. Disaster Risk Reduc.* 40, 101148. doi:10.1016/j.ijdrr.2019.101148

Satriano, C., Elia, L., Martino, C., Lancieri, M., Zollo, A., and Iannaccone, G. (2011). PRESTo, the earthquake early warning system for southern Italy: Concepts, capabilities and future perspectives. *Soil. Dyn. Earthq. Eng.* 31, 137–153. doi:10.1016/j.soildyn.2010.06.008

Seo, J., Lee, J., Lee, H., Jeon, I., Lee, J., and Ahn, J. K. (2021b). Method for determining real-time alarm for local target earthquake early warning using mechanical learning (in Korean). *Korean Patent* 10-221818.

Seo, J., Lee, J., Lee, W., Lee, S., Lee, H., Jeon, I., et al. (2021a). Deep learning-based, real-time, false-pick filter for an onsite earthquake early warning (EEW) system. *J. Earthq. Eng. Soc. Korea* 25, 71–81. doi:10.5000/EESK.2021.25.2.071

Spallarossa, D., Kotha, S. R., Picozzi, M., Barani, S., and Bindi, D. (2019). On-site earthquake early warning: A partially non-ergodic perspective from the site effects point of view. *Geophys. J. Int.* 216, 919–934. doi:10.1093/gji/ggy470

Strauss, J. A., and Allen, R. M. (2016). Benefits and costs of earthquake early warning. *Seismol. Res. Lett.* 87, 765–772. doi:10.1785/0220150149

Vaiciulyte, S., Novelo-Casanova, D. A., Husker, A. L., and Garduño-González, A. B. (2022). Population response to earthquakes and earthquake early warnings in Mexico. *Int. J. Disaster Risk Reduc.* 72, 102854. doi:10.1016/j.ijdrr.2022.102854

Ventura, C. E., Kaya, Y., and Taale, A. (2019). "BC earthquake early warning system, a program for seismic structural health monitoring of infrastructure," in *Seismic isolation, structural health monitoring, and performance based seismic design in earthquake engineering* (Berlin, Germany: Springer), 131–143. doi:10.1007/978-3-319-93157-9_4

Verros, S. A., Wald, D. J., Worden, C. B., Hearne, M., and Ganesh, M. (2017). Computing spatial correlation of ground motion intensities for ShakeMap. *Comput. Geosci.* 99, 145–154. doi:10.1016/j.cageo.2016.11.004

Wang, J. P., Tang, X. S., Wu, Y. M., and Li, D. Q. (2018). Copula-based earthquake early warning decision-making strategy. *Soil Dyn. Earthq. Eng.* 115, 324–330. doi:10.1016/j.soildyn.2018.08.031

Wu, Y. M., and Mittal, H. (2021). A review on the development of earthquake warning system using low-cost sensors in Taiwan. *Sensors* 21, 7649. doi:10.3390/s21227649

Yanwei, W., Xiaojun, L., Zifa, W., Jianping, S., and Enhe, B. (2021). Deep learning for P-wave arrival picking in earthquake early warning. *Earthq. Eng. Eng. Vib.* 20, 391–402. doi:10.1007/s11803-021-2027-6

Yeung, M., Sala, E., Schönlieb, C. B., and Rundo, L. (2022). Unified focal loss: Generalising dice and cross entropy-based losses to handle class imbalanced medical image segmentation. *Comput. Med. Imaging Graph.* 95, 102026. doi:10.1016/j.compmedimag.2021.102026

Zhang, J., and He, S. (2020). Smart technologies and urban life: A behavioral and social perspective. *Sustain. Cities. Soc.* 63, 102460. doi:10.1016/j.scs.2020.102460

Zhou, Y., Yue, H., Kong, Q., and Zhou, S. (2019). Hybrid event detection and phasepicking algorithm using convolutional and recurrent neural networks. *Seismol. Res. Lett.* 90, 1079–1087. doi:10.1785/0220180319

Zhu, L., Peng, Z., McClellan, J., Li, C., Yao, D., Li, Z., et al. (2019). Deep learning for seismic phase detection and picking in the aftershock zone of 2008 M7.9 Wenchuan Earthquake. *Phys. Earth Planet. Inter.* 293, 106261. doi:10.1016/j.pepi.2019.05.004

Zollo, A., Colombelli, S., Elia, L., Emolo, A., Festa, G., and Iannaccone, G. (2014). "An integrated regional and on-site earthquake early warning system for southern Italy: Concepts, methodologies and performances," in *Advanced technologies in Earth Sciences* (Berlin, Heidelberg: Springer), 117–137.